Available online at www.sciencedirect.com
SCIENCE DIRECT®
Journal of Nuclear Materials 340 (2005) 1–11
journal of nuclear materials
www.elsevier.com/locate/jnucmat

Temperature effects on the static and dynamic fracture behaviors of low-silicon CA-15 tempered stainless steel castings

Cheng-Hsun Hsu [a,*], Hwei-Yuan Teng [b]

[a] Department of Materials Engineering, Tatung University, 40 Chungshan North Road, 3rd Sec., Taipei 10451, Taiwan, ROC
[b] Department of Mechanical Engineering, De Lin Institute of Technology, No. 1, Lane 380, Ching-Yun Road, Tu-Cheng, Taipei, Taiwan (236), ROC

Received 7 April 2003; accepted 5 October 2004

Abstract

In this research we studied the effect of testing temperature on both static and dynamic fracturing behaviors of low-silicon CA-15 martensitic stainless steel (MSS) castings after austenitizing and tempering treatments. The results showed that the material's microstructure was influenced by heat treatment and various testing temperatures would cause different fracturing mechanisms. In static tensile tests, the 573–673 K tempered specimens occurred secondary strengthening at 423 K and 298 K testing temperatures. However, there is a contrast of weakening occurred at 123 K for the same type of tempered samples. The phenomenon was mainly triggered by local cracking at the ferrite/martensitic interface and incoherent precipitate site in the materials because of the existence of shrinkage stress under subzero temperature. In the dynamic strain-rate tests, impact embrittlement occurred in the 573–673 K tempered samples as a result of the tempered martensite embrittlement (TME) phenomenon. The ductile-to-brittle transition temperature (DBTT) of the tempered material was obviously lower than that of the as-cast material. Also, optical microscopy (OM), scanning electron microscopy (SEM) and transmission electron microscopy (TEM) were performed to correlate the properties attained to the microstructural observation.

PACS: 81.05.−t; 81.40.−z; 81.70.−q

1. Introduction

Martensitic stainless steel (MSS) possesses excellent strength and corrosion resistance, and can be used in nuclear power plants for pipe material applications that must withstand varying temperatures [1–3]. CA-15 MSS is a cast grade stainless steel that has similar corrosion resistance to that of wrought AISI 410 and 403 MSS. The advantage of the cast material is that it is easy to make into complex components, but segregation and inclusions can reduce its usefulness. In general, cast MSS can be heat-treated by austenitization and tempering processes, which can moderately improve its mechanical and corrosion properties. Unfortunately, a loss in corrosion resistance and mechanical properties can occur after unsuitable tempering treatments [4]. It is common knowledge that a metallic microstructure, chemical composition, the type of heat treatment, and the service

* Corresponding author. Tel.: +886 2 2586 6410; fax: +886 2 2591 7954.
E-mail addresses: chhsu@ttu.edu.tw (C.-H. Hsu), tenghu@dlit.edu.tw (H.-Y. Teng).

0022-3115/$ - see front matter © 2004 Elsevier B.V. All rights reserved.
doi:10.1016/j.jnucmat.2004.10.004

environment generally dominate the fracturing behaviors of the material. Some sources in the literature [5–12] have reported on the mechanical properties and microstructure of wrought MSS that have been produced by heat treatment. However, there have been only a few reports [13,14] related to the mechanical properties of CA-15 castings used at room temperature. Therefore, it is our goal to further study the effects of the testing temperature on the static and dynamic fracturing behaviors of low-Si-modified CA-15 cast samples of a similar grade to AISI 403 MSS, that had been austenitized at 1283 K, air cooled, and then tempered at the temperatures ranging from 573 to 873 K.

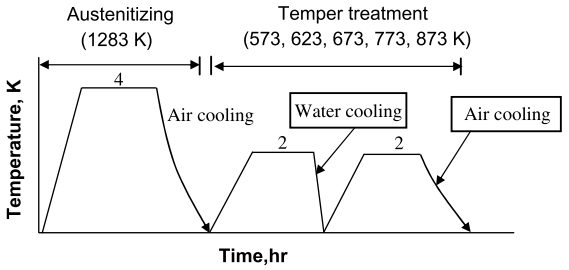

Fig. 3. Schematic illustration for heat treatment conditions in this experiment.

2. Experimental procedures

2.1. Material and specimen preparation

The experimental material was cast in 18 mm Y-blocks using regular foundry practices (Fig. 1). The silicon content was kept below 0.5 mass%, similar to AISI 403 grade MSS. The chemical composition of the material was analyzed by glow discharge spectrometer (GDS). The cast steel was then cut, in preparation for the heat treatment and specimen testing. Tensile and impact tests were performed to examine the static and dynamic fracturing behaviors, respectively. Specimens for tensile testing were machined according to the pin-load tensile testing ASTM E-8M standard [15], which is shown in Fig. 2(a). Impact testing specimens were prepared according to the Charpy V-notch ASTM E-23 standard (Fig. 2(b)) [16].

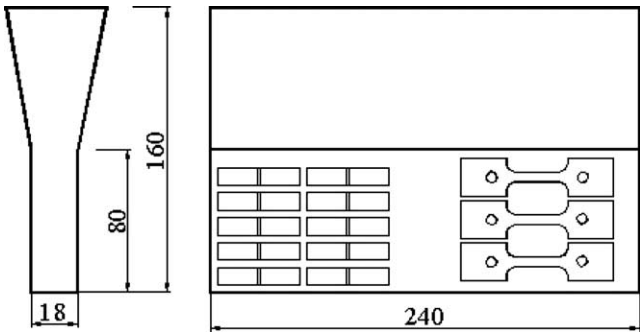

Fig. 1. Dimensions of Y-block casting and location of specimens in the casting.

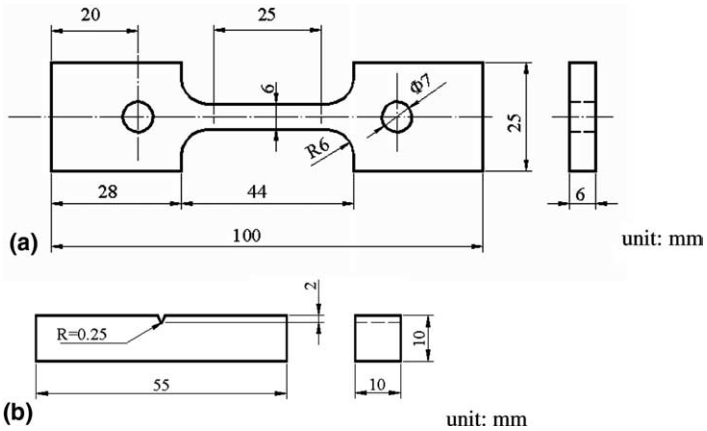

Fig. 2. Dimensions of the specimens for, (a) tensile testing; (b) impact testing.

Table 1
Chemical composition of AISI 403, CA-15 and the experimental material (mass%)

	C	Mn	Si	Cr	P	S	Ni	Fe
AISI 403	0.15 max	1.0 max	0.5 max	11.5–13.0	0.04 max	0.03 max	–	Bal.
CA-15	0.15 max	1.0 max	1.5 max	11.5–14.0	0.04 max	0.04 max	1.0 max	Bal.
As-cast	0.14	0.83	0.34	12.1	0.017	0.001	0.98	Bal.

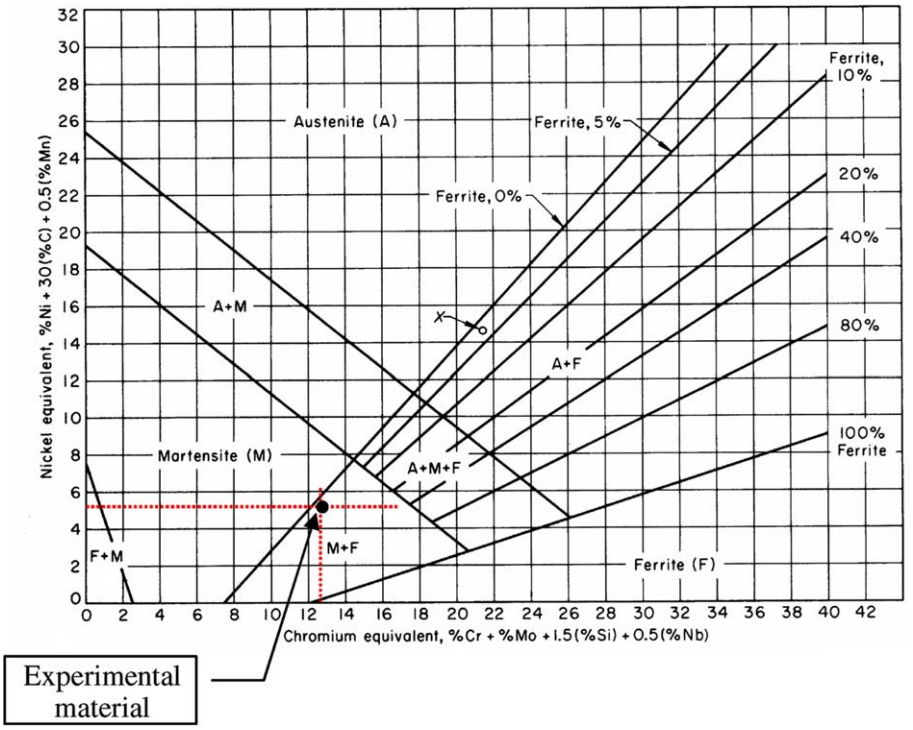

Fig. 4. The microstructure estimated of experimental material by Schaeffler diagram.

2.2. Heat treatment

The heat treatment procedure used in this study is illustrated in Fig. 3. This process involves the following austenitizing and tempering treatments:

(1) The specimens were austenitized at 1283 K for 4 h, then air-cooled.
(2) The specimens were then double tempered at 573, 623, 673, 723 and 823 K, respectively. The specimens were quenched in water after the first tempering for 2 h, and air-cooled after the second tempering for 2 h.

2.3. Microstructural analysis

Optical microscopy (OM), scanning electron microscopy (SEM) and electron probe microanalysis (EPMA) were utilized to examine the material's microstructure. The specimens were polished and etched with Vilella's reagent (5 ml HCl + 1 g Picric + 100 ml ethanol). The SEM was also applied to observe the fracture surfaces

Fig. 5. Constituent averaged amounts of the as-cast microstructure are about 10 ferrite (white area) and 90% martensite (gray area), respectively.

of the tensile and impact specimens for fractography evaluation. In addition, transmission electron microscopy (TEM) and electron diffraction pattern (EDP) were used to identify the precipitates for tempered specimen.

2.4. Hardness testing

Hardness testing of the constituents and bulk sample was performed using the Vickers (100 g) and Rockwell hardness testers, respectively. All the Rockwell hardness readings were converted to a Vickers hardness number. The specimens were polished and etched in the same way as for the metallographic examination before the constituent hardness testing. Five hardness readings were taken and averaged for each heat-treatment.

2.5. Static tensile and dynamic impact tests

All of the static tensile tests were performed using a tensile testing machine (MTS model 810) and tested at a constant strain-rate value, $\dot{\varepsilon} = 10^{-3}\,s^{-1}$. A heating furnace or cooling chamber was attached to the MTS machine for the 423 and 123 K tests, respectively.

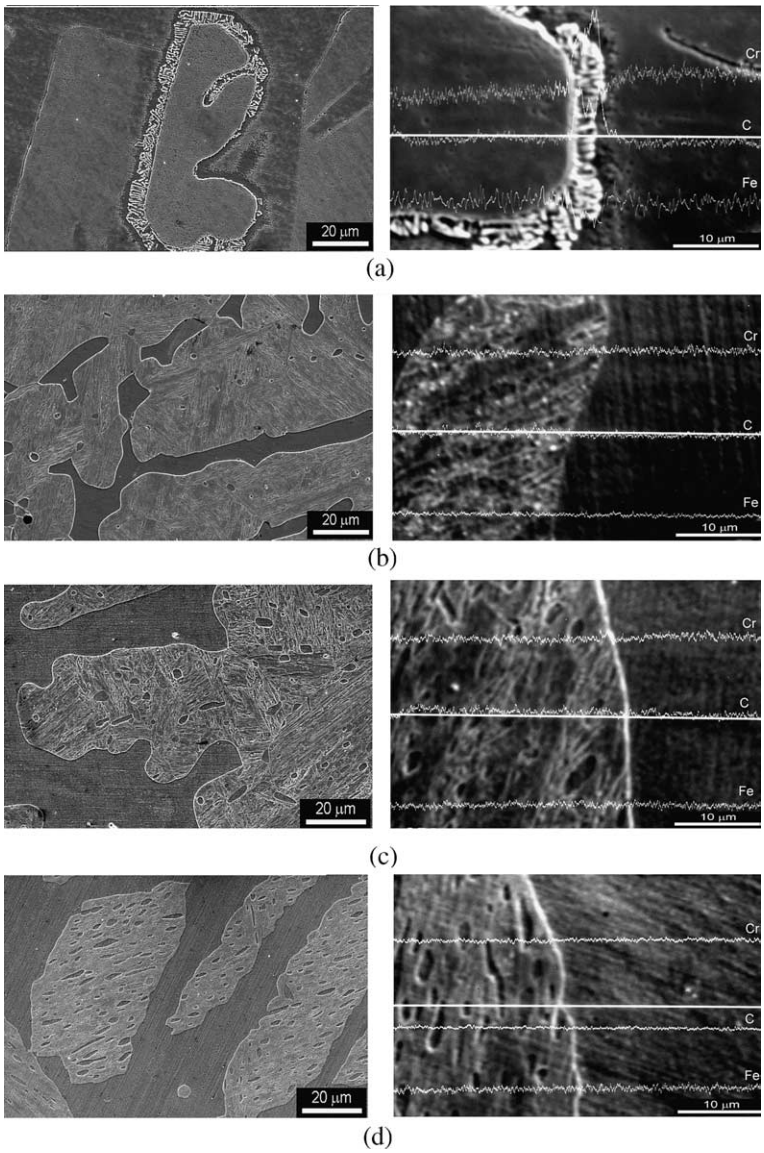

Fig. 6. SEM and EPMA metallography of the experimental materials (a) as-cast, (b) austenitized, (c) tempered at 673 K, (d) tempered at 873 K.

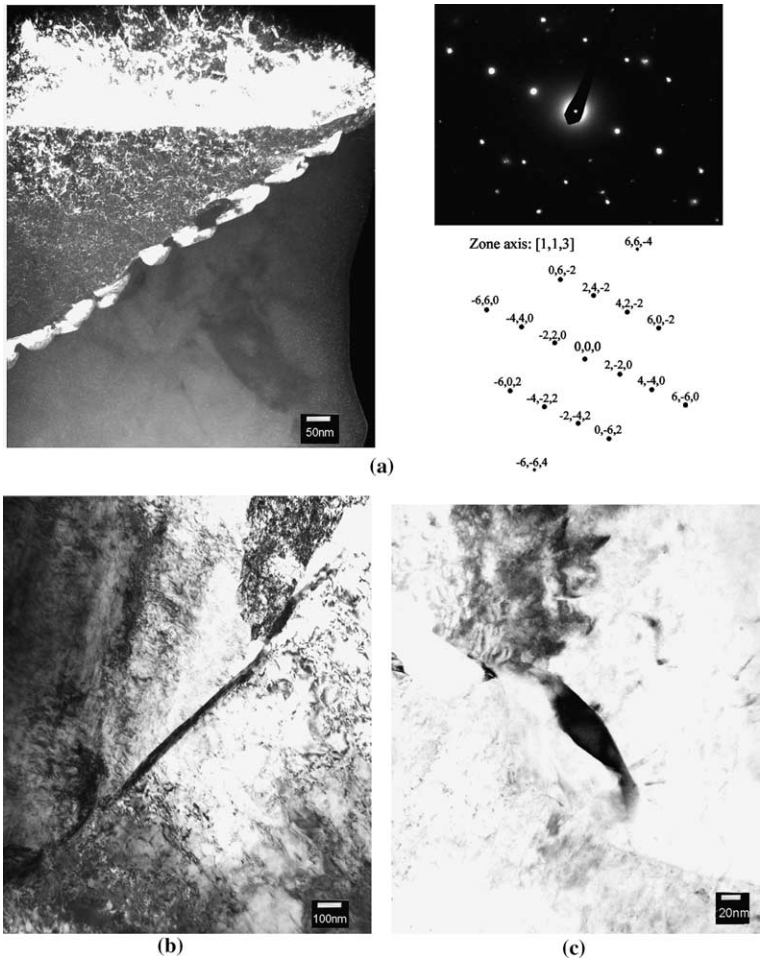

Fig. 7. TEM micrograph and EDP of the carbide precipitated in sample tempered at 673 K: (a) beaded-like carbide, (b) stringed-like carbide, (c) single particle carbide.

Table 2
Hardness (Hv) of specimens for the resulting materials

Heat treatment	Phase in the matrix		Bulk
	Ferrite	Martensite	
As-cast	215	347	289
Austenitized at 1283 K–4 h	239	413	322
Tempered-473 K	226	383	316
Tempered-573 K	247	426	354
Tempered-623 K	248	486	370
Tempered-673 K	263	446	344
Tempered-773 K	259	359	296
Tempered-873 K	189	320	252

Dynamic impact testing, $\dot{\varepsilon} = 10^3\,s^{-1}$, was carried out using a Charpy impact tester. The impacted specimens were respectively immersed in an air furnace and oil bath container for testing at 523, 423, and 348 K, in ice water for testing at 273 K, in dry ice and alcohol for testing at 203 K, and in liquid nitrogen for testing at 77 K. Three tests were done and the results averaged for each condition.

3. Results and discussions

3.1. Chemical composition and microstructure

The chemical composition of the experimental material is listed in Table 1, and compared with AISI 403 and CA-15 MSS. The Ni- and Cr-equivalent values of this material calculated by using Schaeffler [17] formula are 5.435 and 12.61, respectively. According to both of the equivalents in Schaeffler diagram [17] as shown in Fig. 4, it can be seen that microstructure of the experimental material mainly consists of the mixture of martensite and ferrite phases. In this work, the amount of microstructural constituents was measured by using

the software of Optimas/Optimate version 6.2. Fig. 5 shows the as-cast microstructure containing approximately the average amounts of 10% ferrite and 90% martensite and the result is accordant with the above Schaeffler diagram (Fig. 4). Further, SEM and EPMA higher magnification micrographs of the as-cast and heated samples are showed in Fig. 6(a)–(d). In Fig. 6(a), it can be clearly seen that there are Cr-rich precipitates segregating at the martensite/ferrite interface (grain boundary) during casting solidifying process, these precipitates were evaluated and determined to be $Cr_{23}C_6$, similar to those observed in the AISI 403 stainless steel made by Miao [10]. Moreover, the carbides can be eliminated by austenitization of 1283 K–4 h in the work (Fig. 6(b)). Fig. 6(c) shows the micrograph of the sample tempered at 673 K. The microstructure has no obvious change, but the chromium content seems to have a little increase at the grain boundary in EPMA micrograph. Furthermore, the ferritic islands started to generate in the martensitic grains. After tempering at 773 K and 873 K, the Cr-rich precipitates were not appeared. Fig. 6(d) shows the micrographs of sample tempered at 873 K, it has been found that the more ferritic islands produced in the martensitic grains.

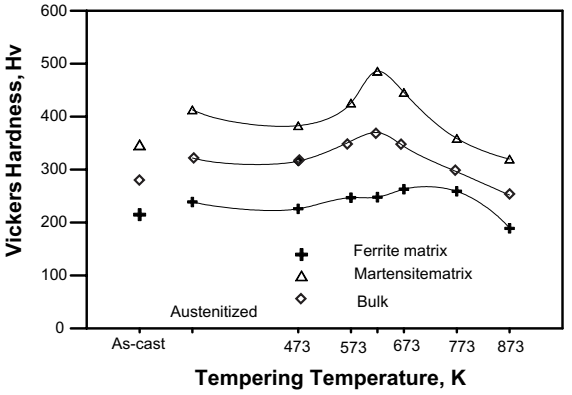

Fig. 8. Effect of tempering temperature on hardness of the specimens.

The TEM micrographs and EDP of 673 K tempered sample are shown in Fig. 7(a)–(c). It can be found that the beaded-like, stringed-like and single-particle precipitates were precipitated at the grain boundary. The precipitates identified from EDP were the $M_{23}C_6$ type carbide. The effects of these microstructural variations on the mechanical properties were further discussed in the following sections.

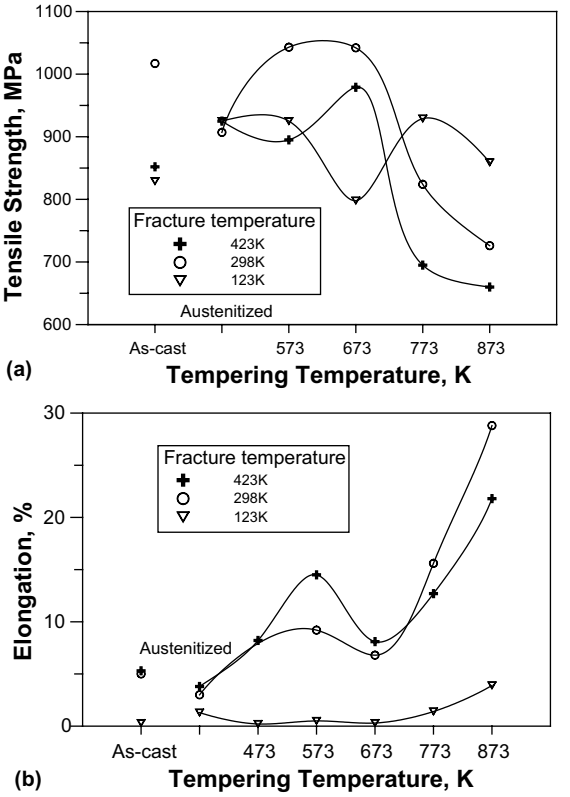

Fig. 9. Effects of tempering and testing temperatures on the tensile properties of the material (a) tensile strength, (b) elongation.

Table 3
Static tensile properties of specimen for the resulting materials

Testing temperature	423 K		298 K		123 K	
Tensile property	UTS (MPa)	Elongation (%)	UTS (MPa)	Elongation (%)	UTS (MPa)	Elongation (%)
As-cast	852	5.3	1017	5.0	829	0.3
Austenitized at 1283 K–4 h	925	3.8	907	3.0	925	1.3
Tempered-473 K	856	8.2	846	7.9	833	0.2
Tempered-573 K	895	14.5	1043	9.2	925	0.5
Tempered-673 K	979	8.1	1042	6.8	798	0.3
Tempered-773 K	695	12.7	824	15.6	926	1.4
Tempered-873 K	660	21.8	726	28.8	859	3.9

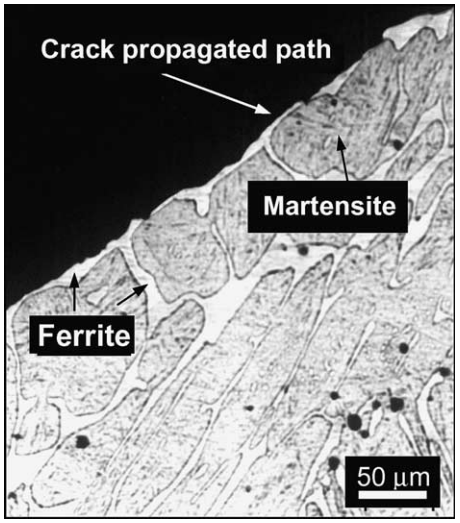

Fig. 10. Metallographic side view of the specimen tempered at 673 K and tensile fractured at 423 K.

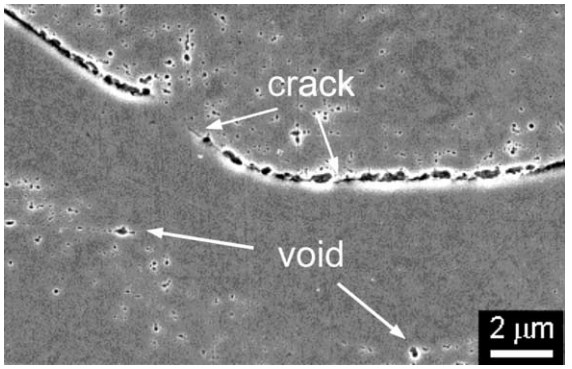

Fig. 11. The SEM micrographics of the 673 K tempered sample immersed into liquid nitrogen.

3.2. Hardness analysis

Table 2 and Fig. 8 show hardness variety of the microstructural constituents in samples tempered at different temperatures. The hardness of the sample austenitized at 1283 K for 4 h was higher than that of the as-cast sample. This is since the chromium carbide at the grain boundary of as-cast sample was re-dissolved into the matrix after austenitization that caused the hardness increase of the material. In addition, tempering effect on hardness is as following changes. The hardness slightly reduced after tempering of 473 K resulting from martensite phase staring to decompose. After tempering of the temperature ranging between 573 K and 673 K, a secondary hardening effect was produced (about at 623 K) by formation of alloy carbides around the grain boundary, as shown in Fig. 7. After 773 K or 873 K high-temperature tempering, the hardness of the material descended speedily, mainly resulting from the softening of the martensite constituent. Also, it was found that the hardness trend of the martensite was similar to the macro-hardness (bulk) trend. In contrast, secondary hardening was non-apparent in the ferrite, being delayed until 773 K. This is why ferritic hardening could have been caused by spinodal decomposition [6]. The hardness of both martensite and ferrite reduced during the 873 K tempering.

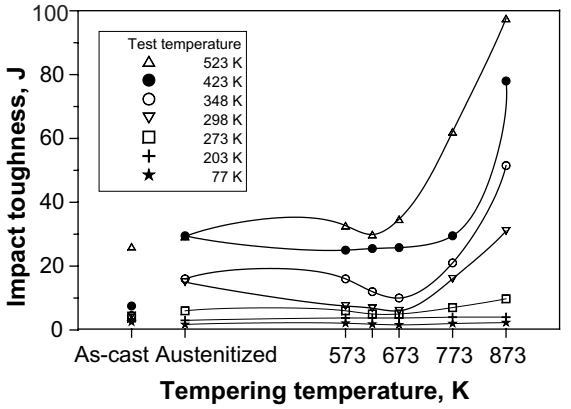

Fig. 12. Effects of tempering and testing temperatures on impact toughness of the material.

3.3. Static tensile behavior

The tensile properties of the as-cast and heat-treated specimens tested at 423, 298 and 123 K, respectively, are

Table 4
Dynamic impact toughness (J) of specimen for the resulting materials

Testing temperature	523 K	423 K	348 K	298 K	273 K	203 K	77 K
As-cast	26.1	7.5	4.5	4.5	3.8	3.5	2.5
Austenitized	29.3	29.5	16	15.0	6	3	1.7
Tempered-573 K	32.7	25.0	16	7.5	6	3.8	2.1
Tempered-623 K	29.9	25.5	12	6.8	5	3.8	1.8
Tempered-673 K	34.7	25.8	10	6.0	5	3.8	1.6
Tempered-773 K	62.1	29.5	21	16.0	7	4	2.0
Tempered-873 K	97.6	78.0	51.5	31.0	9.8	4	2.3

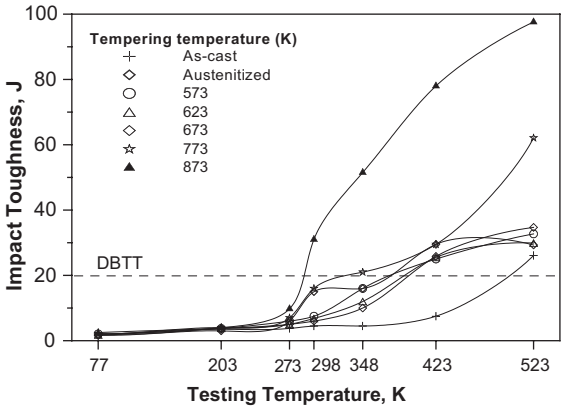

Fig. 13. Comparison of the trend of DBTT for the resulting materials.

listed in Table 3, and the results were compared in Fig. 9. It can be seen that tensile strength of the austenitized specimen was lower than that of the as-cast specimen at room temperature. The carbides had been eliminated by the austenitization of 1283 K–4 h, resulting in an increase of the hardness of the matrix, but the ability that the micro-crack propagation retarded by carbides during the tension was lost simultaneously. A secondary strengthening phenomenon of the material evidently occurred in the specimens tempered at 673 K under the both testing temperatures of 298 K and 423 K (Fig. 9(a)). The reason is that the hardening effect of martensite phase and the re-precipitated carbides retarded tensile micro-cracking connections, resulting in detour of the cracking path and increasing the tensile stress. However, due to the tempered martensite embrittlement (TME) effect, the ductility of the material was also obviously reduced, as shown in Fig. 9(b). Fig. 10 shows a metallographic side view of a specimen tempered at 673 K and then tensile tested at 423 K, and indicates the fracturing path along the location of ferrite phase. The tensile strength of specimens tested at 423 K was lower than those tested at room temperature, which can be explained by a screw dislocation slide at the intermediate temperature, as has also been reported by

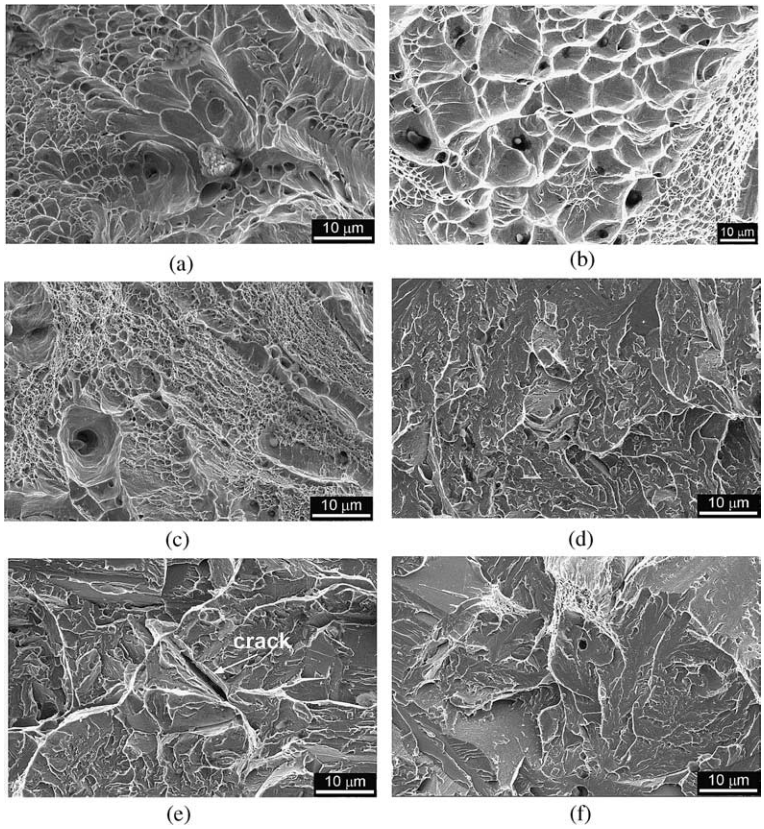

Fig. 14. SEM fractographs: (a) austenitized at 1283 K and tensile fractured at 423 K, (b) tempered at 673 K and tensile fractured at 423 K, (c) tempered at 873 K and tensile fractured at 423 K, (d) austenitized at 1283 K and tensile fractured at 123 K, (e) tempered at 673 K and tensile fractured at 123 K, (f) tempered at 873 K and tensile fractured at 123 K.

Marmy [7]. The strength of the high temperature tempered samples was reduced as a result of matrix softening.

The tensile strength of specimens tested at 123 K showed a distinctly different tendency than that of those tested at 298 K and 423 K. For the specimens tempered at 773 and 873 K, the strength when tested at 123 K was clearly better than that when tested at 298 and 423 K. However, it is important to note that the phenomenon did not occurred in the samples tempered at 673 K. That is, the strength of the 673 K tempered sample had decreased greatly under the subzero testing circumstance (123 K) and was lower than that at 298 and 423 K testing temperatures. This result is similar to the research by Ripling [18]. For further exploring this phenomenon in the work, we have immersed the unstressed 673 K tempered sample into subzero environment (liquid nitrogen) and examined the microstructure by SEM. It was interesting to be found that there are cracking and void occurred in the vicinity of precipitates as shown in Fig. 11. This cause is possible that shrinkage stress produced under subzero temperature resulted in tearing the interface of precipitate and matrix. In addition, all of the experimental specimens in this work had extremely low elongation ($\leqslant$3.9%) at 123 K.

3.4. Dynamic impact behavior

The effect of the tempering temperature on impact toughness of the material at the different testing temperatures is showed in Fig. 12 and Table 4. The results showed that impact values of the tempered materials under the intermediate and room temperatures (298–523 K) have a similar trend, in which the brittleness phenomenon occurred at tempering temperature range of 573–673 K. The materials with carbides precipitated at the martensite/ferrite interface (as in the as-cast and 673 K tempered specimens) experienced rapidly cracking connection and tearing under dynamic strain-rate fracturing, and the toughness was reduced evidently. Fig. 13 shows a comparison of the ductile–brittle transition temperature (DBTT), defined as a 20 J energy criterion

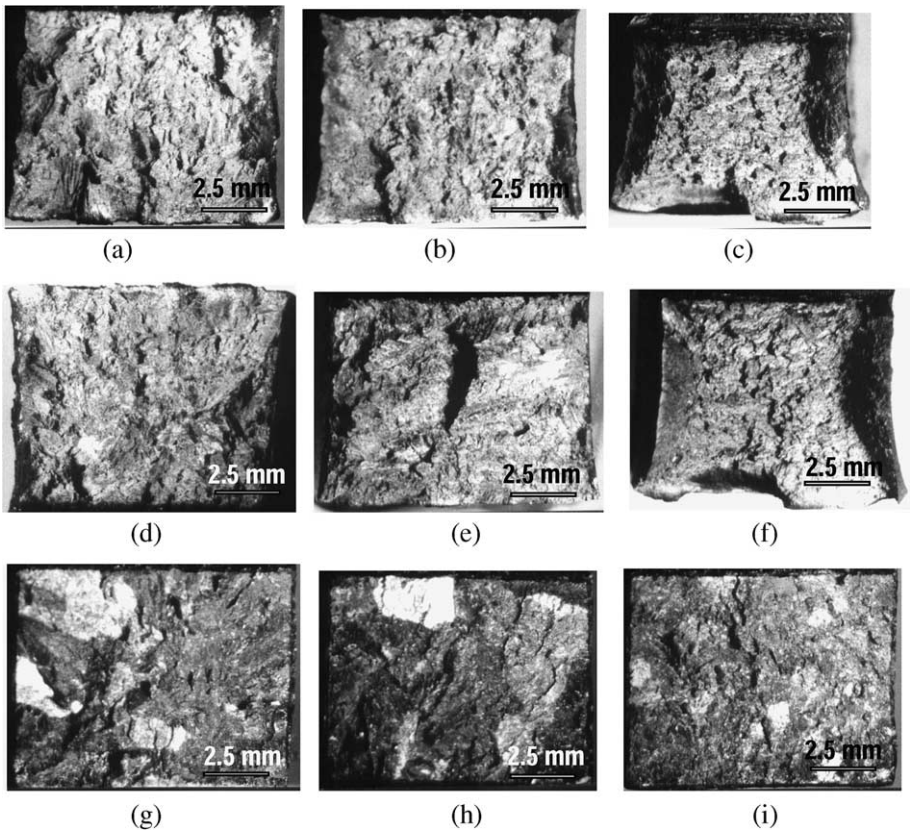

Fig. 15. Fracture surfaces of Charpy impact specimens: (a) austenitized and fractured at 523 K, (b) tempered at 673 K and fractured at 523 K, (c) tempered at 873 K and fractured at 523 K, (d) austenitized and fractured at 423 K, (e) tempered at 673 K and fractured at 423 K, (f) tempered at 873 K and fractured at 423 K, (g) austenitized and fractured at 77 K, (h) tempered at 673 K and fractured at 77 K, (i) tempered at 873 K and fractured at 77 K.

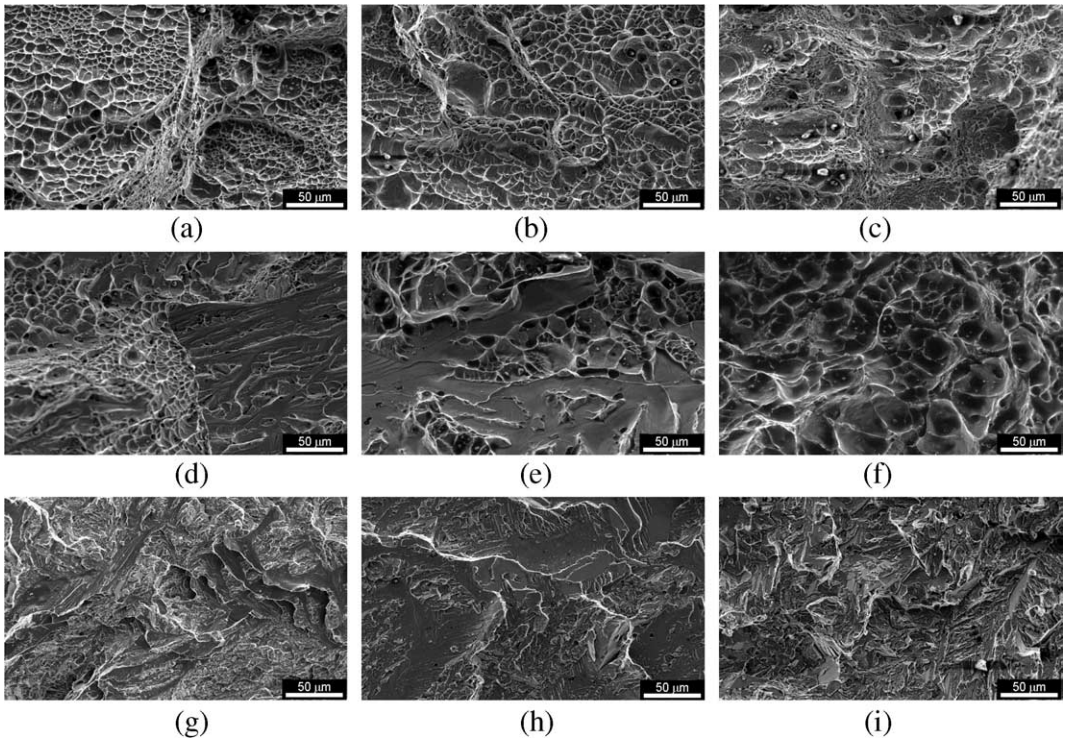

Fig. 16. SEM fractographs of Charpy impact fracture appearance: (a) austenitized and fractured at 523 K, (b) tempered at 673 K and fractured at 523 K, (c) tempered at 873 K and fractured at 523 K, (d) austenitized and fractured at 423 K, (e) tempered at 673 K and fractured at 423 K, (f) tempered at 873 K and fractured at 423 K, (g) austenitized and fractured at 77 K, (h) tempered at 673 K and fractured at 77 K, (i) tempered at 873 K and fractured at 77 K.

[19], of the experimental materials in the work. The results showed that the DBTT of all heat-treated specimens was lower than that of the as-cast specimen; in particular, the higher tempering temperature for the material could show the distinct improvement on DBTT. Also, the impact toughness increased with the increase of the testing temperature.

3.5. Fractography

SEM fractographs of the tensile specimens fractured at 423 and 123 K are illustrated in Fig. 14. The mixed features of micro-void coalescence, herringbone pattern and little dimples can be found in austenitized specimen fractured at 423 K (Fig. 14(a)). The features of larger micro-void coalescent intergranular fracture and local smaller dimples occurred in 673 K tempered specimen fractured at 423 K (Fig. 14(b)). Contrastively, the ductile fractured morphology with more dimple features was observed in 873 K tempered specimen tested at 423 K (Fig. 14(c)). Both brittle cleavage and river patterns are quite apparent in Fig. 14(d)–(f), which were heat-treated specimens tested at 123 K. In particular, the crack initiation can be found in the 673 K tempered sample fractured at 123 K.

Figs. 15 and 16 respectively illustrate the macroscopic and microscopic fractographs of specimens fractured by Charpy impact test at various testing temperatures. From these figures, it can be seen that no plastic deformation existed in specimens fractured at subzero temperatures (Fig. 15(g)–(i)). The fractographs of these specimens typically show the brittle fracture morphology with large cleavage facets and river patterns. On the other hand, there was large-scale plastic deformation occurred in the 873 K tempered specimen tested at 423 K (Fig. 15(f)). The fractography of the specimen primarily showed dimple features, as shown in Fig. 16(f), representing the ductile fracturing morphology and thus produced better impact toughness. Also, the austenitized and 673 K tempered specimens fractured at 423 K, showed a little plastic deformation (Fig. 15(d) and (e)), and had the mixture of ductile (dimple) and brittle (cleavage) fracture modes (Fig. 16(d) and (e)).

4. Conclusions

In this research we evaluated the influence of the tempering and testing temperatures on the static and

dynamic fracturing behavior of low-silicon CA-15 castings. The following conclusions can be made:

(1) As-cast microstructure of the material consisted of martensite and ferrite constituents and there were chromium carbides precipitated at the ferrite/martensitic interface. These precipitates could be eliminated by austenitization at 1283 K for 4 h, which resulted in the increase of the material's hardness. When the austenitized material was then tempered at the range of 573 and 673 K, there was a secondary hardening phenomenon occurred because the martensite constituent decomposed into tempered martensite and tiny carbides. In the case of tempering at 773 and 873 K, the Cr-rich carbides were not re-precipitated and thus both constituents of martensite and ferrite in the microstructure were softer.

(2) In the static tensile behavior, when the material tempered at 673 K and respectively tested at 298 and 423 K, it possessed the greatest tensile strength (secondary strengthening), but there was simultaneously a TME phenomenon resulting in the decrease of the ductility at the same tempering and testing conditions. The strengths of the specimens tempered at 773 and 873 K and fractured at 123 K were higher than those fractured at 198 and 423 K. However, the secondary strengthening of the materials did not occur in the subzero environment (123 K). On the contrary, the strength decreased greatly. This cause is possible that shrinkage stress produced under subzero temperature resulted in tearing and cracking the precipitate/matrix interface. In addition, all of the experimental specimens had extremely low elongations ($\leqslant 3.9\%$) at 123 K testing temperature.

(3) In terms of the dynamic impact behavior, both the intermediate and room temperature tests showed a similar trend, wherein brittleness occurred in 623–673 K tempering range. The DBTT of the heat-treated specimens was lower than that of the as-cast specimen. Samples tempered at high temperatures were especially obvious. Moreover, the impact toughness increased with the increase of the testing temperature.

Acknowledgments

The authors would like to express their sincere thanks for the financial support of the National Science Council (Taiwan, ROC) under Contract No. NSC 89-2216-E-036-020.

References

[1] J.S. Dubey, S.L. Wadekar, J.K. Chakravartty, J. Nucl. Mater. 254 (1988) 271.
[2] P.R. Sreenivasan, S.K. Ray, S.L. Mannan, P. Rodriguez, J. Nucl. Mater. 228 (1996) 338.
[3] M.D. Mathew, L.M. Lietzan, K.L. Murty, V.N. Shah, Mater. Sci. Eng. A269 (1999) 186.
[4] L.C. Lim, M.O. Lai, J. Ma, D.O. Northwood, B. Miao, Mater. Sci. Eng. A171 (1993) 13.
[5] J.J. Shiao, C.H. Tsai, J.J. Kai, J.H. Huang, J. Nucl. Mater. 217 (1994) 269.
[6] L. Devillers-Guerville, J. Besson, A. Pineau, Nucl. Eng. Des. 168 (1997) 211.
[7] P. Marmy, J.L. Martin, M. Victoria, Mater. Sci. Eng. A164 (1993) 159.
[8] L. Shi, D.O. Northwood, Acta. Metall. 43 (2) (1995) 453.
[9] G. Gupta, J.S. Dubey, S. Ganguly, A.R. Bisway, Y.V. Kamart, J.K. Chakravartty, High Temp. Mater. Process. 16 (1) (1997) 65.
[10] B. Miao, D.O. Northwood, L.C. Lim, M.O. Lai, Mater. Sci. Eng. A171 (1993) 21.
[11] M. Rieth, B. Dafferner, J. Nucl. Mater. 233–237 (1996) 229.
[12] L. Schafer, M. Schirra, K. Ehrlich, J. Nucl. Mater. 233–237 (1996) 264.
[13] ASM Metal Handbook, Heating Treating 4, 1991, p. 785.
[14] ASM Metal Handbook, Properties and Selection: Iron, Steels, and High-performance Alloys, 1, 1990, p. 698.
[15] ASTM E 8M-97, Standard test methods for tension testing of metallic materials, 03.01. 1997, p. 77.
[16] ASTM E 23-96, Standard test methods for notched bar impact testing of metallic materials, 03.01. 1996, p. 137.
[17] R.A. Lula, Stainless Steel, ASM, 1993, p. 109.
[18] E.J. Ripling, Trans. ASM 42 (1950) 439.
[19] R.W. Hertzberg, Deformation and Fracture Mechanics of Engineering Materials, Wiley, 1996, p. 375.